Exact gravitational dual of a plasma ball

JHEP08(2009)012

(http://iopscience.iop.org/1126-6708/2009/08/012)

Published by IOP Publishing for SISSA

Received: *June 9, 2009*
Accepted: *July 21, 2009*
Published: *August 6, 2009*

Exact gravitational dual of a plasma ball

Roberto Emparan[a,b] **and Giuseppe Milanesi**[c]

[a] *Institució Catalana de Recerca i Estudis Avançats (ICREA), Passeig Lluís Companys, 23, E-08010 Barcelona, Spain*
[b] *Departament de Física Fonamental, Universitat de Barcelona, Marti i Franquès 1, E-08028 Barcelona, Spain*
[c] *Departament ECM, Universitat de Barcelona, Marti i Franquès 1, E-08028 Barcelona, Spain*

E-mail: emparan@ub.edu, milanesi@ecm.ub.es

Abstract: We present an exact solution for a black hole localized near an infrared wall in four-dimensional anti-deSitter space. By computing the holographic stress tensor we show that the CFT dual of the black hole is a 2+1-dimensional ball (i.e., a disk) of plasma at finite temperature, surrounded by vacuum. This confirms some earlier conjectures about plasma balls in AdS/CFT. We also estimate the value of the surface tension for the ball. The solution displays a number of peculiarities, most notably a non-trivial curvature of the boundary geometry, as well as other properties associated to the vanishing deconfinement temperature of the set up. We discuss how these features are related to specific physics at the infrared and ultraviolet boundaries for this solution, and should not be generic properties of plasma balls.

Keywords: Black Holes in String Theory, AdS-CFT Correspondence, Black Holes

ArXiv ePrint: 0905.4590

doi:10.1088/1126-6708/2009/08/012

JHEP08(2009)012

Contents

JHEP08(2009)012

1 Introduction

It has been shown recently that the Einstein equations that describe the dynamics of black holes in anti-deSitter space can be recast, when the length scales involved are much larger than the cosmological radius, in the form of the equations of a relativistic conformal fluid [1]. This is likely to advance our understanding of both of these apparently different physical systems. An interesting extension of this correspondence involves fluids with surface boundaries. Such is the case of plasmas in quantum field theories with a confinement first order phase transition, where balls of deconfined plasma surrounded by the confining vacuum can form slightly above the deconfinement temperature.

Gravitational duals for such plasma balls are expected in theories of anti-deSitter gravity that admit solutions for homogeneous black branes and solutions with an 'infrared bottom', i.e., a limit to the inward extent away from the boundary in the Poincaré patch of AdS. Plasma balls were discussed in detail in this context in [2], mostly within a purely gravitational realization of dual confinement, but the phenomenon is expected to be present largely independently of the details of the infrared cutoff. It was argued that the gravitational dual of plama balls should be black holes in the bulk, localized near the infrared end of spacetime. Their horizon should be 'pancaked' and well approximated by a black brane in the

region away from the interface with the infrared end. The correspondence has been subsequently exploited in [3] in order to reveal properties of hitherto unknown black holes in AdS that exhibit behavior remarkably similar to black holes in asymptotically flat spacetime.

This correspondence between plasma balls and black holes remains, however, conjectural in some of its aspects. The gravity/fluid correspondence has been proven in [1] only for plasma fluids without surface boundaries, since at the plasma boundary the density and pressures vary rapidly and the hydrodynamic description breaks down. Thus the dual bulk physics of the surface boundary requires solving the full gravitational equations and the approximations in [1] are not valid. Ref. [2] obtained a numerical solution for an infinite planar interface between the AdS-soliton (confined) and black brane (deconfined) phases. But so far no solution for a black hole dual to a *finite* plasma ball has been shown to exist.[1] Our purpose is to present and discuss an exact solution that describes such an object.

To this end, we use a previously known exact solution for an accelerating black hole in four-dimensional AdS. Our construction can be regarded as the complement of the one in [5] for a black hole localized in an ultraviolet brane. In ref. [5], the spacetime for a black hole moving in an accelerated trajectory inside AdS was cut off in a Randall-Sundrum II braneworld construction, throwing away the region from the brane to infinity — the ultraviolet.[2] In the present paper we will instead retain this region and cut out its complement — the infrared. This crude procedure provides the simplest way to implement an infrared cutoff. We shall show that the black holes we construct give rise to several of the properties conjectured for the dual plasma balls — actually plasma disks, since they live in 2+1 dimensions.

The solutions also display certain peculiarities related in one way or another to the conditions imposed at the infrared bottom and at asymptotic infinity. The way we introduce the infrared end by effectively breaking spontaneously the conformal symmetry gives rise to a number of subtleties, which affect the properties of the deconfinement transition and possibly also the shape of the black hole horizon. At the opposite end, we encounter issues that relate to the asymptotic behavior of the solutions. The black hole solutions in AdS_4 that we use were originally found by looking for metrics in an algebraically special class (Petrov type-D) instead of specifying any particular kind of asymptotics. Thus we find a somewhat unconventional behavior of the geometry at the asymptotic AdS boundary, which however may turn out to have an interesting interpretation.

Our main objective in this paper is to establish the main features of the black holes localized in the infrared and of their plasma ball duals. We do this in sections 2 and 3. The subtleties of boundary conditions are discussed in section 4. However, since they are somewhat secondary to our initial purpose here, they are not dealt with in full detail. Pursuing these interesting matters further is left for future work.

[1] Ref. [4] obtained some information on infrared black holes using linearized gravity around an AdS infrared brane background.

[2] This and other related solutions have subsequently been used as exact models for other configurations relevant to the cutoff AdS/CFT correspondence [6–8].

JHEP08(2009)012

2 The exact solution

Our starting point is a subfamily of a class of solutions to Einstein's equations with a negative cosmological constant in four dimensions first presented in [9]. We discuss it succintly, since more details can be found in [5].[3] The metric is

$$ds^2 = \frac{\ell^2}{(x-y)^2}\left[-\ell^{-2}H(y)dt^2 + \frac{dy^2}{H(y)} + \frac{dx^2}{G(x)} + G(x)d\phi^2\right] \tag{2.1}$$

with

$$H(y) = y^2(1+2\mu y)\,, \qquad G(x) = 1 - x^2 - 2\mu x^3\,. \tag{2.2}$$

Here $\ell = \sqrt{-3/\Lambda}$ is the cosmological radius. The solution contains a single dimensionless parameter μ. We take it to lie in the range

$$0 < \mu < \mu_c \equiv \frac{1}{3\sqrt{3}}\,, \tag{2.3}$$

so that $G(x)$ has three real roots x_0, x_1, x_2 satisfying

$$-\frac{1}{2\mu} < x_0 < x_1 < 0 < x_2\,. \tag{2.4}$$

Other parameter ranges are either equivalent or do not give the physics we seek. Although it is customary in the literature to use μ as the parameter for this family of solutions, we have found much more practical to use instead the root x_1, in terms of which

$$\mu = \frac{1-x_1^2}{2x_1^3} \tag{2.5}$$

and

$$x_0 = x_1\frac{1+\sqrt{4x_1^2-3}}{2(x_1^2-1)}\,, \qquad x_2 = x_1\frac{1-\sqrt{4x_1^2-3}}{2(x_1^2-1)}\,. \tag{2.6}$$

The range (2.3) and the ordering (2.4) are reproduced when

$$x_{1c} \equiv -\sqrt{3} < x_1 < -1\,. \tag{2.7}$$

The upper limit $x_1 \to -1$ corresponds to $\mu \to 0$, in which case the coordinate transformation

$$x = -\frac{\ell - z}{\sqrt{r^2+(\ell-z)^2}}\,, \qquad y = -\frac{\ell}{\sqrt{r^2+(\ell-z)^2}} \tag{2.8}$$

brings the solution into the form of the Poincaré patch of empty AdS_4

$$ds^2 = \frac{\ell^2}{z^2}\left(dz^2 - dt^2 + dr^2 + r^2 d\phi^2\right) \tag{2.9}$$

($-\ell/y$ and $\arccos(x)$ are polar coordinates in the plane (r,z) centered at $(0,\ell)$). The opposite, 'critical' limit $x_1 \to x_{1c}$ corresponds to the upper bound on $\mu \to \mu_c$ in which the black hole becomes, in a specific way that we explain below, of infinite size.

[3] The use of this solution to construct black holes on an infrared brane was first discussed in [5]. Another reference using this idea is [10] but our analysis differs very substantially from it.

JHEP08(2009)012

If we demand that $G(x) > 0$ so that x and ϕ are spatial coordinates, then we must require that x lies in the range $x_1 \leq x \leq x_2$. We will shortly restrict this range further to incorporate the infrared cutoff.

It is easily seen that there is an event horizon at $y = -1/(2\mu)$, and a curvature singularity at $y = -\infty$. The range of y outside the horizon is $-1/(2\mu) < y < x$. Asymptotic infinity lies at $y = x$. The temperature of the horizon, normalized relative to the Killing vector ∂_t, is

$$T = \frac{1}{8\pi\mu\ell}\,. \tag{2.10}$$

The locus $x = x_1$ is a semi-axis of rotation (a fixed-point set) for ∂_ϕ, which extends from the horizon towards asymptotic infinity. In order to avoid a conical singularity there we identify $\phi \sim \phi + \Delta\phi$, with

$$\Delta\phi = \frac{4\pi}{G'(x_1)} = \frac{4\pi x_1}{x_1^2 - 3}\,. \tag{2.11}$$

Observe that $\Delta\phi > 2\pi$ and that it diverges as $x_1 \to -\sqrt{3}$. The canonically normalized angular variable is

$$\tilde{\phi} = \frac{x_1^2 - 3}{2x_1}\phi\,. \tag{2.12}$$

with $\tilde{\phi} \sim \tilde{\phi} + 2\pi$. This identification introduces a conical excess-angle singularity along the opposite semi-axis $x = x_2$. Physically, this line singularity is interpreted as a 'strut' that pushes the black hole and keeps it in a trajectory that accelerates towards the boundary of AdS. We shall eliminate this singularity by removing the portion of AdS where it lies.

Indeed, we are interested in introducing an infrared cutoff in AdS space. We shall implement this by cutting off the space at a surface whose extrinsic curvature is proportional to its induced metric. Such a cutoff can be regarded as due to a 'wall' or 'infrared brane' with a distributional source of energy-momentum of vacuum type. These requirements for the infrared cutoff are met at the surface $x = 0$. So we cut off the geometry (2.1) by restricting x to the range

$$x_1 \leq x \leq 0\,. \tag{2.13}$$

In this way we retain the region of AdS from the wall out to infinity. This is most clearly seen when the black hole is absent, $\mu = 0$, where the change (2.8) maps the interval (2.13) of (2.1) to $0 \leq z \leq \ell$ in (2.9). This is in contrast to the construction in [5], where the complement of this region was kept. In the following we shall often refer to this infrared cutoff as 'the brane' even if we do not intend to imply any particular connection to braneworld models.

The brane thus introduced has the gravitational effect of a negative-tension domain wall. The unstable negative energy oscillations can be projected out in a conventional manner by imposing 'orbifold' boundary conditions. On the other hand, the infrared cutoff introduces a mass gap $\sim 1/\ell$ in the spectrum of Kaluza-Klein graviton modes.[4] But there

[4]We are using here terminology borrowed from braneworlds, where a Kaluza-Klein-type mode decomposition of fields along the direction z is customarily performed.

JHEP08(2009)012

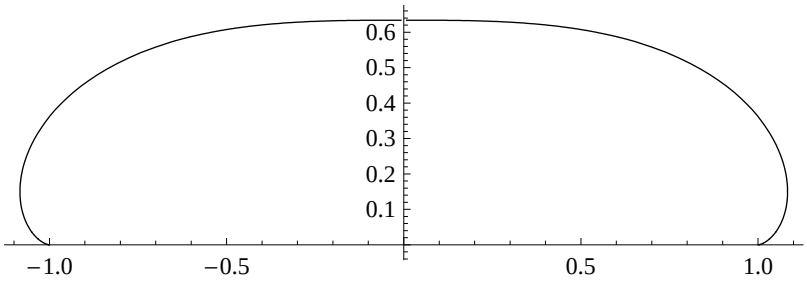

Figure 1. Profile of the black hole localized near the infrared wall exhibiting the 'low-wetting' effect. Shown here is (a polar section of) the embedding in Euclidean 3D space of the horizon geometry, cut off by the infrared brane (which lies along the lower horizontal axis in the figure). The figure corresponds to $\mu = 1/(4\sqrt{2})$ ($x_1 = -\sqrt{2}$). As the black hole grows larger the horizon spreads along directions parallel to the infrared brane, but it also bends over near its edge before touching the brane ('droplet on a plastic sheet'). Units correspond to $\ell = 1$.

is no mechanism to stabilize the location of the brane so there is a massless modulus, the radion, corresponding to its position. In section 4 we discuss further the nature of this cutoff and the effects of the massless radion.

2.1 Horizon geometry

The spatial geometry induced on the horizon at $y = -1/2\mu$ is

$$ds_H^2 = \frac{\ell^2}{(x + 1/(2\mu))^2}\left[\frac{dx^2}{G(x)} + G(x)d\phi^2\right], \tag{2.14}$$

with x within the range (2.13). The coordinate x plays the role of (the cosine of) a polar angle along the horizon, with $x = x_1$ being the pole, i.e., the axis of rotational symmetry, and $x = 0$ the point of contact with the infrared brane. The horizon area is easily computed to be

$$A_H = 4\pi\ell^2 \frac{(x_1^2 - 1)^2}{x_1^2(3 - x_1^2)}. \tag{2.15}$$

This area grows monotonically as μ increases from 0 to μ_c, i.e., x_1 decreases from -1 to $-\sqrt{3}$, and becomes much larger than ℓ^2 as x_1 approaches the critical value $-\sqrt{3}$. The latter is the regime we will be mostly interested in.

This horizon displays what can be described as a *low-wetting effect*. A way to illustrate it pictorially is by drawing the profile of an embedding of the horizon into 3D Euclidean space, see figure 1. For very small μ the horizon is approximately hemi-spherical, with radius $\simeq 2\mu\ell$ much smaller than the AdS radius ℓ. But as μ grows the horizon's circumference is longest at a finite distance away from the brane, like a droplet of water on a plastic surface. The 3D embedding cannot be performed for $x_1 < -\sqrt{2}$ since in that case the intrinsic scalar curvature of the horizon in a region near the rotation axis becomes negative. Nevertheless, the low-wetting can be demonstrated by showing that, for every given value of $x_1 \in (-\sqrt{3}, -1)$, the circumference length of the horizon at latitude x

$$\mathcal{C}(x) = \Delta\phi\sqrt{g^H_{\phi\phi}(x)} \tag{2.16}$$

JHEP08(2009)012

reaches a maximum at a value x_m away from the brane location $x = 0$. In the critical limit $x_1 \to -\sqrt{3}$ the length $\mathcal{C}(x)$ diverges for any $x > x_1$, but the limiting x for the maximum circle approaches $x_m \simeq -0.54$ and the ratio between the maximum circumference of the horizon and the circumference on the brane remains finite[5]

$$\frac{\mathcal{C}(x_m)}{\mathcal{C}(0)} \simeq 1.107 > 1\,. \tag{2.17}$$

This low-wetting effect is presumably related to the specific nature of the infrared cutoff we have imposed and of its interaction with the black hole horizon, which seems to be repulsive. This is in spite of the fact that the negative-tension brane attracts objects in the bulk. The latter can be regarded as the reason why the horizon flattens along the brane, and is expected for any kind of infrared cutoff. However, we do not find any reason why the low-wetting effect should be generic for the horizons of duals of plasma balls.

A more striking feature is the appearance of a region of negative curvature around the center of the horizon. A better understanding of this important region is obtained from our next analysis.

2.2 Limit to a black brane

Motivated by the dual physical picture of plasma configurations, we expect that as the black hole becomes larger it should approach, in a region around its center (rotation symmetry axis), the geometry of a black brane, which is the dual of the deconfined phase. Something like this does happen in our solution, but with an unexpected twist.

In order to investigate the limit in which the black hole becomes large, $\mu \to \mu_c$, we introduce

$$\mu = \mu_c \left(1 - \frac{\epsilon^2}{2}\right) \tag{2.18}$$

for small ϵ, so that

$$x_0 = x_{1c} - \epsilon + O(\epsilon^2)\,, \qquad x_1 = x_{1c} + \epsilon + O(\epsilon^2)\,, \qquad x_2 = \frac{\sqrt{3}}{2} + \frac{\epsilon^2}{12\sqrt{3}} + O(\epsilon^3)\,. \tag{2.19}$$

Furthermore, to focus on the geometry near the rotation axis of the horizon $x = x_1$ and away from the edges, we define a coordinate ξ,

$$x = x_{1c} + \epsilon \cosh \xi\,. \tag{2.20}$$

that remains finite as $\epsilon \to 0$. It is also convenient to introduce a new radial coordinate

$$\varrho = -\frac{\ell}{y + \sqrt{3}}\,. \tag{2.21}$$

The horizon at $y = -3\sqrt{3}/2$ is now mapped to

$$\varrho_H = \frac{2\ell}{\sqrt{3}}\,. \tag{2.22}$$

[5]The exact values for x_m and the ratio can be found but are not too illuminating.

In the limit $\epsilon \to 0$ the solution (2.1) becomes a hyperbolic AdS black hole (also known as 'topological black hole')

$$ds^2 \to -f(\varrho)dt^2 + \frac{d\varrho^2}{f(\varrho)} + \varrho^2 \left(d\xi^2 + \sinh^2\xi\, d\tilde{\phi}^2\right) , \tag{2.23}$$

where

$$f(\varrho) = \frac{\varrho^2}{\ell^2} - 1 - \frac{2m}{\varrho} \tag{2.24}$$

with mass parameter

$$m = \frac{\ell}{3\sqrt{3}} . \tag{2.25}$$

This is different from the black brane ('planar black hole') that naively we might have expected, which would have $f = \frac{\varrho^2}{\ell^2} - \frac{2m}{\varrho}$ and a planar horizon. Nevertheless, this geometry is also dual to a deconfined phase of the CFT, with the deconfined degrees of freedom contributing a large entropy (dual to the Bekenstein-Hawking entropy).

Hyperbolic black holes approach planar black holes when they are very large, $m \gg \ell$. However we are not in this regime since in the present case m is of the same order as ℓ.[6] Observe also that the temperature remains finite in this limit. Naively one would have expected it to approach the deconfinement temperature, which, as we discuss in section 4, is zero for this model. These are indications that, although the horizon area diverges as $\mu \to \mu_c$, there is a sense in which the black hole is not spreading indefinitely along the infrared wall. The growing lengths and areas in the geometry are a result of the coalescence of two roots of $G(x)$, x_0 and x_1, which make the periodicity $\Delta\phi$ and the proper distance along the polar direction, $dx/\sqrt{G(x)}$, grow unbounded. But observe in particular that the latter diverges in the region near the pole $x \approx x_1$, and not near the edge $x \approx 0$. In this sense the black hole horizon does not extend to arbitrarily large distances along the brane. Rather, its central area is warping to become a hyperbolic horizon.

In summary, our black hole localized near the infrared wall demonstrates some of the properties anticipated for such solutions on general grounds, but also a number of peculiarities that were less expected. In the next section we turn to the holographic dual description, which shows again both kinds of aspects from a different perspective.

3 The plasma ball

3.1 Boundary geometry and holographic stress tensor

The properties of the CFT state dual to our black hole can be conveniently derived by writing the metric in Fefferman-Graham coordinates (z, x^i) in which

$$ds^2 = \frac{\ell^2}{z^2}\left(dz^2 + g_{ij}(z,x)dx^i dx^j\right) . \tag{3.1}$$

[6] In fact the mass is precisely that for which $f(\varrho)$ has a double zero at $\varrho = -\ell/\sqrt{3}$ (inside the event horizon), $f(\varrho) = \frac{\ell}{\varrho}\left(\frac{\varrho}{\ell} + \frac{1}{\sqrt{3}}\right)^2\left(\frac{\varrho}{\ell} - \frac{2}{\sqrt{3}}\right)$. While we do not have any physical explanation for this particular value, one could anticipate it since the function $f(\varrho)$ is essentially the same as $H(y)$, and $H(y)$ has a double zero at $y = 0$ i.e., $\varrho = -\ell/\sqrt{3}$.

JHEP08(2009)012

When the metric g_{ij} is expanded in power series of z,

$$g_{ij}(z,x) = \sum_{n=0}^{\infty} g_{ij}^{(n)}(x)\, z^n\,, \tag{3.2}$$

the leading term $g_{ij}^{(0)}$ corresponds to (a representative of the conformal class of) the metric at the boundary. Given $g_{ij}^{(0)}$ the Einstein equations fix the terms $g_{ij}^{(1)}$ and $g_{ij}^{(2)}$ but $g_{ij}^{(3)}$ contains information about the particular state of the solution at hand [11, 12]. More specifically, it gives the renormalized stress tensor of the dual theory as

$$\langle T_{ij}(x)\rangle = \frac{3\ell^2}{16\pi G} g_{ij}^{(3)}(x)\,. \tag{3.3}$$

We defer the details of the calculation to the appendix, and quote here only the final results. In order to reduce clutter we set $\ell = 1$ in eqs. (3.4)–(3.7).

The boundary metric is

$$g^{(0)} = -\frac{1+x_1^2\rho}{x_1^2(1+\rho)}dt^2 + \frac{(1+\rho)^4}{\rho(1+x_1^2\rho)(3-x_1^2+3\rho+\rho^2)}d\rho^2 + \frac{\rho(3-x_1^2+3\rho+\rho^2)}{x_1^2(1+\rho)}d\phi^2\,. \tag{3.4}$$

The coordinate ρ runs from 0 to ∞ and when $x_1 = -1$ it is related to r in (2.9) as $r = \sqrt{\rho(\rho+2)}$. Although ρ does not correspond to any invariant notion of radius it is a convenient coordinate for keeping expressions as simple as possible.

The holographic stress tensor is

$$\begin{aligned}
\langle T_t^t\rangle &= \frac{1}{16\pi G}\frac{x_1^2-1}{(1+\rho)^3}\left(-3\frac{1+x_1^2\rho}{(1+\rho)^3}+1\right)\,,\\
\langle T_\rho^\rho\rangle &= \frac{1}{16\pi G}\frac{x_1^2-1}{(1+\rho)^3}\,,\\
\langle T_\phi^\phi\rangle &= \frac{1}{16\pi G}\frac{x_1^2-1}{(1+\rho)^3}\left(3\frac{1+x_1^2\rho}{(1+\rho)^3}-2\right)\,.
\end{aligned} \tag{3.5}$$

This stress tensor must be traceless and conserved, $g_{ij}^{(0)}\langle T^{ij}\rangle = 0$ and $\nabla_i\langle T^{ij}\rangle = 0$ [12]. We have explicitly checked that these properties hold.

The first thing to observe is that the boundary metric is not flat. More precisely, since the Cotton tensor of $g^{(0)}$ does not vanish the conformal class of the boundary metric is not flat. Perhaps more strikingly, we get a different boundary metric for each value of x_1. In the usual AdS/CFT interpretation, this means that in the bulk there are not only normalizable excitations of the graviton, which give rise to $\langle T_{ij}\rangle$, but also non-normalizable gravitational modes which deform the boundary geometry. Since our solutions only have one parameter, x_1, we cannot change independently the normalizable and non-normalizable contributions. Thus, the stress tensor $\langle T_{ij}\rangle$ that we obtain for each bulk black hole corresponds to a state of the dual CFT living in a different background spacetime. We will comment on a possible alternative view of this effect in section 4.

The metric near the origin is

$$g^{(0)} \to -\frac{dt^2}{x_1^2} + \frac{1}{3-x_1^2}\frac{d\rho^2}{\rho} + \frac{3-x_1^2}{x_1^2}\rho d\phi^2 \qquad (\rho \approx 0)\,. \tag{3.6}$$

JHEP08(2009)012

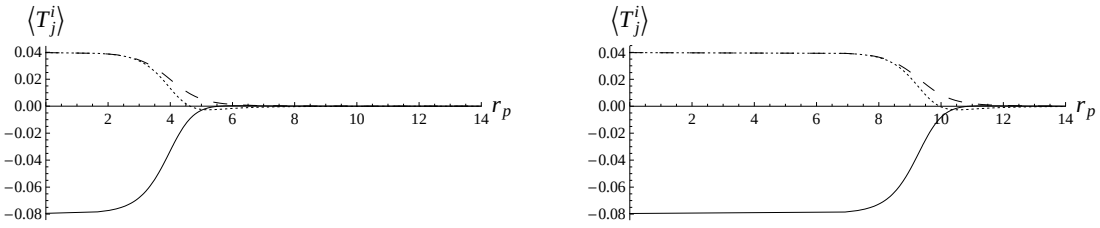

Figure 2. Holographic stress tensor components $\langle T^t_t \rangle$ (solid), $\langle T^\rho_\rho \rangle$ (dashed), $\langle T^\phi_\phi \rangle$ (dotted) of the plasma ball as a function of proper radial distance r_p. Left: $x_1 = x_{1c} + 10^{-3}$. Right: $x_1 = x_{1c} + 10^{-7}$. As x_1 approaches x_{1c} the conformal thermal fluid relations $\langle T^t_t \rangle : \langle T^\rho_\rho \rangle : \langle T^\phi_\phi \rangle = -2 : 1 : 1$ hold to great accuracy in a larger region. The entropy of the dual black hole can be reproduced by the entropy of a step-function homogenous plasma that would extend out to $r_p = 4.16$ (left), $r_p = 9.48$ (right). Units correspond to $\ell = 1$, $G = 1$.

The change $\rho = \tilde{\rho}^2/4$ reveals more clearly that this is a flat metric when the periodicity of ϕ is fixed to (2.11) in order to avoid a conical singularity at the origin. This has the consequence that the metric near infinity

$$g^{(0)} \to -dt^2 + \frac{1}{x_1^2}\left(d\rho^2 + \rho^2 d\phi^2\right) \qquad (\rho \to \infty)\,, \tag{3.7}$$

is only locally asymptotically flat: it asymptotes to a cone with excess angle $\Delta\phi - 2\pi > 0$. Observe also that the origin is redshifted by a factor $1/|x_1| < 1$ relative to infinity.

In order to characterize the radial profile of the configuration we shall use, as an appropriate invariant quantity, the proper radial distance

$$r_p = \int_0^\rho d\rho' \sqrt{g^{(0)}_{\rho\rho}(\rho')}\,. \tag{3.8}$$

Even if $g^{(0)}_{\rho\rho}$ diverges at $\rho = 0$ in (3.6), this is simply a coordinate artifact and for $x_{1c} < x_1 < -1$ the proper radius r_p runs from 0 at $\rho = 0$ out to infinity as $\rho \to \infty$. We could also work with the circumferential radius $\sqrt{g^{(0)}_{\phi\phi}(\rho)}\,\Delta\phi/2\pi$, but this contains a strong distortion from the divergence of $\Delta\phi$ as $x_1 \to -\sqrt{3}$.

To demonstrate the presence of the plasma ball we plot in figure 2 the stress tensor as a function of proper radius r_p. At the center of the ball we have

$$\langle T^i_j(r_p = 0) \rangle = \frac{x_1^2 - 1}{16\pi G\ell}\mathrm{diag}(-2, 1, 1)\,, \tag{3.9}$$

which is of the form of a perfect fluid of thermal conformal radiation. Figure 2 shows that as x_1 approaches the critical limit these central values for the energy densities and pressures remain almost constant out to a large radial distance, and then drop fairly rapidly to zero. This is the profile expected for a ball of plasma.

There are, however, some peculiarities to this configuration of the dual CFT that are the boundary counterpart of our previous result that as horizons become large they develop a negatively curved region around their rotation axis. The scalar curvature $R^{(0)}$ for the

JHEP08(2009)012

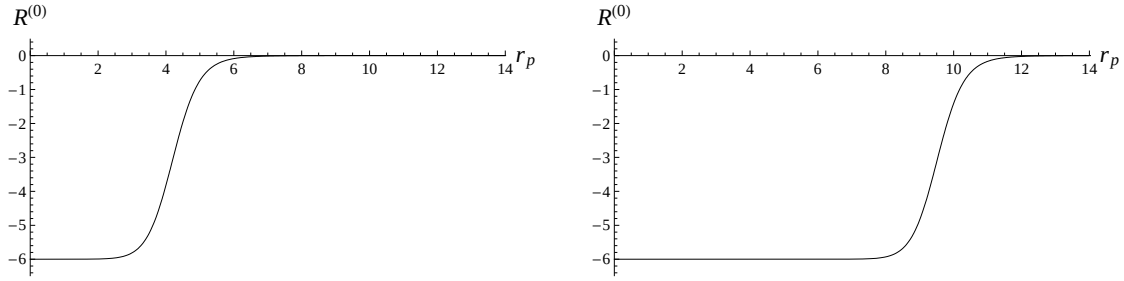

Figure 3. Scalar curvature $R^{(0)}$ of the boundary geometry as a function of proper radial distance r_p. Left: $x_1 = x_{1c} + 10^{-3}$. Right: $x_1 = x_{1c} + 10^{-7}$. The plasma of figure 2 lies within the region of almost uniform scalar curvature $R^{(0)} \simeq -6$. Units correspond to $\ell = 1$.

boundary metric $g^{(0)}$ is negative. Figure 3 shows that as x_1 approaches the critical limit there is a large region around the center with almost uniform negative scalar curvature, which then turns fairly rapidly into an almost flat region that extends to infinity.

The region where the plasma resides coincides very approximately with this region of negative scalar curvature $R^{(0)} \approx -6\ell^{-2}$. This is expected, given that the black brane limit of the bulk black hole, i.e., the dual of the deconfined phase, yields a hyperbolic black hole. Indeed we can take the boundary counterpart of the limit in section 2.2 with (2.19) and

$$\rho = \epsilon \frac{2}{\sqrt{3}} \sinh^2 \frac{\xi}{2} \tag{3.10}$$

to find that

$$g^{(0)} \to \frac{1}{3}\left(-dt^2 + d\xi^2 + \sinh^2 \xi d\tilde{\phi}^2\right) \tag{3.11}$$

and

$$\langle T^i_j \rangle \to \frac{1}{8\pi G\ell} \mathrm{diag}\,(-2, 1, 1) \ . \tag{3.12}$$

The stress tensor for the hyperbolic black hole of (2.23), with the mass given by (2.25), is $1/3^{3/2}$ of (3.12) [13]. The difference is accounted for by the conformal factor $1/3$ in front of (3.11), which is due to a slightly different choice of the Fefferman-Graham coordinate z than would be natural for the metric (2.23). Taking this into account, it follows that the temperature of the plasma ball is equal to the Hawking temperature of the black hole in the bulk (2.10).

It is also curious to observe that outside the ball $\langle T^t_t \rangle$ and $\langle T^\phi_\phi \rangle$ change sign, i.e., there are small negative energy densities and pressures, and in fact asymptotically the ratios $\langle T^t_t \rangle : \langle T^\rho_\rho \rangle : \langle T^\phi_\phi \rangle = 1 : 1 : -2$ are approached.

3.2 Size and shape of the plasma ball

We may now try to approximate the plasma ball by a step-function distribution of homogeneous plasma with stress tensor equal to (3.12) extending out to a proper radial distance $r_{\rm ball}$. It is then also possible to assign an entropy to this approximate plasma ball as the local entropy density of the homogeneous plasma times the area in $g^{(0)}$ occupied by the plasma.

JHEP08(2009)012

The entropy density of the homogeneous plasma in (3.12) is computed from the entropy density of the hyperbolic black hole (2.23), which is $\varrho_H^2/(4G\ell^2) = 1/(3G)$, times a factor $3 = (\sqrt{3})^2$ that takes into account the conformal factor in (3.11) relative to the boundary of (2.23) as explained before. This is

$$s_{\rm plasma} = 3\frac{1}{3G} = \frac{1}{G}\,. \tag{3.13}$$

The area that the plasma occupies is

$$A_{\rm ball} = \ell^2 \int_0^{\Delta\phi} d\phi \int_0^{\rho_{\rm ball}} d\rho \, \sqrt{g^{(0)}_{\rho\rho}\, g^{(0)}_{\phi\phi}} \simeq \frac{4\pi\ell^2}{3-x_1^2}\rho_{\rm ball}\,, \tag{3.14}$$

for x_1 close to $x_{1c} = -\sqrt{3}$. We may now fix the coordinate radius of the ball $\rho_{\rm ball}$ so that the plasma entropy

$$S_{\rm ball} \simeq s_{\rm plasma} A_{\rm ball} \simeq \frac{4\pi\ell^2}{G}\frac{\rho_{\rm ball}}{3-x_1^2} \tag{3.15}$$

reproduces the Bekenstein-Hawking entropy of the bulk black hole. From (2.15) the latter is

$$S_{\rm BH} = \frac{A_H}{4G} \simeq \frac{4\pi\ell^2}{3G}\frac{1}{3-x_1^2}\,, \tag{3.16}$$

again for $x_1 \simeq x_{1c}$. Thus demanding that $S_{\rm ball} \approx S_{\rm BH}$ fixes

$$\rho_{\rm ball} \approx \frac{1}{3}\,. \tag{3.17}$$

The (x_1-dependent) value of $r_{\rm ball}$ that follows from this does not admit a simple expression. However, if our definition of it is any reasonable, $r_{\rm ball}$ should bound the region where the profile of the actual plasma is almost constant. Numerical inspection (see figure 2) reveals that the proper radial extent of the ball, $r_{\rm ball}$, for the coordinate radius (3.17) coincides very approximately with the point at which either of the components of $\langle T^i_j\rangle$, as a function of r_p, has an inflection point

$$\left.\frac{d^2\langle T^i_j\rangle}{dr_p^2}\right|_{r_p=r_{\rm ball}} \approx 0\,. \tag{3.18}$$

This shows that the approximation of the plasma ball as an almost-homogeneous distribution of plasma is indeed sensible.

It is easy to see that the area occupied by the plasma ball, and its proper radial extent out to $r_{\rm ball}$, grow unbounded near the critical limit. However, in parallel with what we found for the bulk horizon, this does not mean that the plasma ball extends out to infinity. Since $\rho_{\rm ball}$ remains finite as $x_1 \to x_{1c}$, it follows that the divergence of the proper radius $r_{\rm ball}$ in this limit is not due to an unbounded growth of the distance from any point in the ball out to its edge. Rather, as eq. (3.6) makes clear, what happens is that the radial distance from any point *to the origin*,

$$r_p \simeq 2\ell\sqrt{\frac{\rho}{3-x_1^2}} \qquad (\rho \approx 0), \tag{3.19}$$

JHEP08(2009)012

diverges as $x_1 \to -\sqrt{3}$. This is, the geometry around the origin develops a trough within which the plasma ball lies, and this trough gets deeper as x_1 approaches x_{1c}.

So it is not quite accurate to say that in this limit the ball spreads out to larger radii in the surrounding vacuum. A more precise way to express this is through the trace of the extrinsic curvature K of the circle at the ball radius.[7] In the limit $x_1 \to x_{1c}$ this curvature at the ball's outer circumference remains finite,

$$K|_{r_p=r_{\rm ball}} \to \sim 1.5\ell^{-1} \tag{3.20}$$

so the edge of the ball always remains a circle of finite curvature and does not approach the shape of a straight domain-wall.

Thus the region occupied by the plasma does become arbitrarily large but only within the negatively-curved trough. The transition region between vacuum and plasma phases has thickness of order ℓ, which could be expected, but this is also the scale of other characteristic lengths of the ball. In particular the extrinsic curvature radius at $r_{\rm ball}$, and also the thermal length of the plasma and the intrinsic curvature radius of the background are always of the same order $\sim \ell$. So we never are really in the hydrodynamic regime where variations of the plasma occur on scales much longer than the thermal wavelength.

Usually the stress tensor of large plasma balls can be effectively split into a volume term of deconfined plasma (as above) and a boundary term with a surface tension σ. The fluid equations then relate, very generally, the pressure drop across the surface to its extrinsic curvature through the Young-Laplace equation

$$P = \sigma K\,. \tag{3.21}$$

Despite the fact that we never reach the hydrodynamic regime where K and the ball's intrinsic curvature are much smaller than the temperature, it may still be useful to assign a surface tension to these balls through eq. (3.21). Taking P to be the value at the center of the ball, $P = 1/8\pi G\ell$, and K as in (3.20), we obtain

$$\sigma \simeq 0.026 G^{-1} \simeq 0.07 \frac{\epsilon}{T}\,, \tag{3.22}$$

where in the last expression ϵ and T are the energy density and temperature of the plasma. Given the uncertainties involved, these numbers should not be trusted much more than as estimations of order of magnitude.

4 Discussion: physics of the infrared and ultraviolet boundaries

Let us recapitulate the salient aspects of our study in section 3. Figure 2 illustrates our claim that the duals of the black hole solutions (2.1) can be regarded as plasma balls. However certain features demand further explanation. Near the critical limit we find large disks of deconfined plasma. But these disks lie within a trough of negative curvature in the 2+1 background geometry, whose size is different for each plasma ball. The trough

[7] The extrinsic curvature is computed for the circle at $r_{\rm ball}$ in the entire spacetime, i.e., not only in a spatial section.

JHEP08(2009)012

gets deeper as the critical limit is approached, but it never extends out to larger distances in the asymptotically flat part of the geometry. Instead the edge of the plasma, with thickness of order ℓ, approaches a circle of finite curvature radius. Related to this, the pressure difference inside and outside the ball does not become arbitrarily small as the ball becomes larger, and the limiting temperature does not seem to admit an interpretation as a deconfinement temperature. In addition, even if deep down the trough the solutions approach a homogeneous plasma configuration, its fluctuations may not admit a proper hydrodynamic description since the thermal wavelength of the plasma is of the same order as the curvature of the background.

In the following we make a number of observations concerning the properties of the ultraviolet and infrared boundaries that we hope help understand several of these issues.

4.1 Asymptotic boundary behavior and dynamical gravity on the boundary

From the perspective of the gravitational bulk, it is worth recalling that the metric (2.1) was found without any special regard for specific boundary conditions. Instead it arose from a general analysis of Petrov type-D metrics of the Einstein-Maxwell theory with a cosmological constant [9]. It is quite possible that other solutions for black holes accelerating in AdS_4 exist with different asymptotic behavior. Physically, this may be realized if the black hole is accelerated by a different, even if more singular, pushing rod, for which the linear energy density and pressure are different from each other and possibly even non-uniform (unlike in a conical singularity where they are equal and uniform). This should certainly modify the asymptotic behavior and conceivably it will allow the existence of solutions for infrared black holes with (conformally) flat boundary metric. Sadly, such metrics cannot be of special algebraic type D, and we do not know of any method that can possibly give them in exact form.[8] Thus, approximate analytic or numerical methods seem to be the best way to investigate them. The latter applies as well to the higher-dimensional cases.

From a viewpoint closer to the AdS/CFT interpretation, it would not be inconsistent to think of the solution as the result of first fixing a μ-dependent boundary geometry $g^{(0)}$ and then solving the gravitational bulk equations for a black hole localized near the infrared cutoff. This would in fact be the conventional interpretation in AdS/CFT in which the boundary metric is not a dynamical field. This is in effect what we have been assuming in section 3. But such a choice of boundary behavior certainly does not appear natural.

Instead, it might appear more natural to think of $g^{(0)}$ as a geometry modified by the presence of the plasma. This would require that the boundary metric becomes a dynamical field. Interestingly, it has been argued recently that dynamical gravity at the AdS boundary can arise by appropriate choice of asymptotic boundary conditions [14, 15]. Namely, the conventional Dirichlet conditions on the graviton lead to non-dynamical gravity, as in standard AdS/CFT, but mixed Dirichlet-Neumann conditions (with an appropriate finite norm for the bulk graviton) can give rise to a suitable gravity theory. In the case of AdS_4

[8] This is in spite of the presence of two commuting abelian isometries in the expected solution. In four dimensions, inverse scattering techniques allow to construct solutions of $R_{\mu\nu} = 0$ for black holes accelerated by more general (and more singular) rods than conical defect lines, but with a cosmological constant the theory is not known to be integrable.

JHEP08(2009)012

the gravitational action is generically expected to contain the Einstein-Hilbert term, a cosmological constant, and a gravitational Chern-Simons term, each with an independent coefficient, and a possible coupling to sources.

The cosmological constant is absent in our solutions with asymptotically (locally) flat $g^{(0)}$, but the other two terms should be present. The Einstein-Hilbert term is a relevant operator and at large distances should dominate the dynamics over the Chern-Simons term, which is marginal and should kick in at shorter distances. Evidence for this comes from the fact that, asymptotically as $\rho \to \infty$, the Einstein equations

$$R^{(0)}_{ij} - \frac{1}{2} g^{(0)}_{ij} R^{(0)} = \frac{8\pi G}{\ell} \langle T_{ij} \rangle \tag{4.1}$$

are satisfied by (3.4) and (3.5) to leading order in $1/\rho$, i.e., to linearized order around (locally) flat space. Observe though that the linearized gravity dynamics implied in (4.1) is not the leading effect at large distances: in (3.4) there is an asymptotic conical angle. The fact that it is an excess angle is suggestive of a repulsive gravitational effect (possibly a negative mass) and perhaps some kind of instability.[9] On the other hand, dynamical gravity on the boundary would make the presence of a conical deficit angle at the origin (which we have barred, but would appear if the asymptotic geometry were globally flat, $\phi \sim \phi + 2\pi$) more acceptable, since it could be caused by a pointlike mass source.

The further investigation of the appropriateness of this interpretation of the curvature of $g^{(0)}$ lies beyond the scope of the present paper, but we find it highly suggestive.

Finally, dynamical gravity helps understand the puzzling issue of what phase transition are these plasma balls associated to: at finite temperature the vacuum would nucleate bubbles of plasma whose self-gravity curves the spacetime that they appear in.

4.2 Massless radion and the deconfinement transition

We have introduced the infrared wall by simply cutting off the spacetime at a surface whose extrinsic curvature is proportional to its induced metric. This is a consistent procedure for creating a mass gap in the graviton spectrum, but observe that since the introduction of this brane does not modify the geometry away from it, it is obvious that it does not affect the asymptotic behavior of the spacetime and does generate any non-vanishing trace $\langle T^i_i \rangle$. Thus conformal symmetry of the dual theory is not explicitly broken. Instead, it is spontaneously broken. As discussed in section 2, the position of the infrared wall in (empty) AdS is a modulus, commonly known as the massless radion, which is the Goldstone boson of the translation symmetry in z that is spontaneously broken by the brane. Hence the holographic dual theory contains a massless field whose vev breaks spontaneously conformal invariance.

The effects of this massless radion on the deconfinement phase transition were investigated in [17]. It was found that at any small temperature the black brane is the dominant phase, i.e., the deconfinement temperature is vanishingly small (neglecting the corrections of a thermally-generated potential for the radion). This is not unexpected since the location of the infrared brane is arbitrary and hence it cannot be said to lie above or below the

[9] Note the low-wetting in section 2.1 also suggests repulsion. Refs. [16] discuss possibly related instabilities of black holes on negative-tension branes

JHEP08(2009)012

horizon of the black brane. Thus we recover essentially the same phase structure as in the conformal theory.

Thus in our set up black branes form at any temperature above zero. There is not a first-order phase transition, since the entropy jump to the plasma phase can be made arbitrarily small (for finite volume) by reducing the temperature. So proper plasma balls in equilibrum in flat spacetime are not expected. Still, fireballs may form, say in high-energy collisions, which would reproduce several of the aspects of a black hole localized in the infrared end (see [4]). However, the ball would not have a surface tension to prevent it from spreading in a flat spacetime and eventually cooling down to arbitrarily small temperature.

The main mechanism that keeps our plasma balls in equilibrium seems to be the curvature of the spacetime that creates a trough within which the plasma lies. We have suggested above that this may be the result of dynamical gravity on the boundary, and in this case the transition might be of first order and thus a surface tension might perhaps be identified as we have done.

In order to introduce a proper confinement/deconfinement phase transition (in a flat non-dynamical background) the location of the infrared wall must be stabilized, i.e., the radion must get a mass, and the deconfinement scale will be set by this mass. Aspects of the phase transition that results have been discussed in [17].

We do not see any easy way in which our solutions for infrared black holes can be modified to accommodate for radion stabilization. Giving a large mass to the radion makes the infrared brane very rigid and this will presumably modify the shape and other properties of the black hole that lies on top of it. In particular the low-wetting effect, which apparently is due to the interaction between the black hole and the infrared brane, could disappear when the dynamics of the latter is modified. The stability properties of the black hole/infrared brane configuration may also be altered.

5 Outlook

Finding new exact solutions for black holes on infrared branes with different boundary behavior than in this paper, or in higher dimensions, seems out of reach at present. Nevertheless, valuable information may be obtained in a linearized approximation in which a specific asymptotic boundary behavior is naturally imposed from the beginning. The study of the linearized approximation to black holes in the infrared was addressed in [4], which actually also considered the effects of radion stabilization on the solutions. It seems possible to us to extend this analysis to gain further information about black holes that approach a brane-like behavior.

Other possible avenues for generalization of our solutions, using again previously known exact metrics in AdS_4, involve rotation and charge on the black holes. These are being currently investigated [18].

JHEP08(2009)012

Acknowledgments

We are grateful to Shiraz Minwalla, Alex Pomarol, Mukund Rangamani and Toby Wiseman for discussions, to Gary Horowitz and Rob Myers for comments on a draft of this paper, and to Alessandro Maccarrone for early collaboration. Part of this work was done while RE enjoyed the warm hospitality of: Niels Bohr Institute; TIFR and ICTS during the 2008 Monsoon Workshop on String Theory in Mumbai; the CERN TH Institute program on Black Holes; and the Cosmophysics group in KEK, Tsukuba. RE was supported by DURSI 2005 SGR 00082, MEC FPA 2007-66665-C02 and CPAN CSD2007-00042 Consolider-Ingenio 2010. GM was supported by MEC FPA 2007-66665-C01 and the ENRAGE Program MRTN-CT-2004-005616.

A Fefferman-Graham expansion of the metric

In this appendix we set $\ell = 1$.

In order to compute the holographic stress tensor we need to write the metric (2.1) in the form

$$ds^2 = \frac{1}{z^2}\left(dz^2 + \sum_{n=0}^{3} z^n\, g_{ij}^{(n)} dx^i dx^j + O(z^4)\right) . \tag{A.1}$$

For our purposes we need not care whether the $O(z^4)$ terms include crossed g_{iz}, or g_{zz} metric components.

We begin by introducing a 'zeroth-order' set of coordinates $(x, y) \to (r_0, z_0)$ through

$$x = \frac{x_1(1-z_0)}{\sqrt{r_0^2 + (1-z_0)^2}}\,, \qquad y = \frac{x_1}{\sqrt{r_0^2 + (1-z_0)^2}} \tag{A.2}$$

(compare to (2.8)). This brings the solution (2.1) into the form (A.1) only when $x_1 = -1$, as there appear non-zero $g_{r_0 z_0}$ components at low orders in z_0. In order to remove these up to order z^3 in an expansion around $z = 0$, we redefine the coordinates

$$z_0 = z + f_2(\rho) z^2 + f_3(\rho) z^3 + f_4(\rho) z^4 + O(z^5)\,, \tag{A.3}$$

$$r_0 = \sqrt{\rho(\rho+2)}\left(1 + g_1(\rho) z + g_2(\rho) z^2 + g_3(\rho) z^3 + g_4(\rho) z^4 + O(z^5)\right) . \tag{A.4}$$

The functions f_n, g_n must vanish when $x_1 = -1$ since this corresponds to empty AdS. We have found convenient to introduce a radial coordinate ρ that looks awkward for empty AdS where $r_0 = \sqrt{\rho(\rho+2)}$ but which simplifies significantly the results for generic x_1.

Plugging the coordinate transformations (A.2), (A.3) and (A.4) in the metric (2.1) and expanding in powers of z, at each order we require first that $g_{z\rho}^{(n)} = 0$ and then $g_{zz}^{(n)} = 0$. In this way g_n and f_n are obtained as solutions of purely algebraic equations, without the

JHEP08(2009)012

need of integrating differential equations. We find

$$
\begin{aligned}
f_2 =& -\frac{x_1^2-1}{2(\rho+1)^3}\,,\\
f_3 =& \frac{x_1^2-1}{16(\rho+1)^6}\left[3(1-4\rho)x_1^2+8(\rho+1)^3-15\right]\,,\\
f_4 =& -\frac{x_1^2-1}{48(\rho+1)^9}\Big[3x_1^4\left(20\rho^2-12\rho+1\right)-6x_1^2\left(10\rho^4+26\rho^3+18\rho^2-28\rho+3\right)+\\
&\qquad +8(\rho+1)^6-84(\rho+1)^3+99\Big]
\end{aligned}
\tag{A.5}
$$

and

$$
\begin{aligned}
g_1 =& \frac{1-x_1^2}{\rho^2+3\rho+2}\,,\\
g_2 =& \frac{x_1^2-1}{2(\rho+1)^4(\rho+2)^2}\left[\rho^4+5\rho^3-\rho^2\left(x_1^2-10\right)-\rho\left(x_1^2-8\right)+x_1^2+1\right]\,,\\
g_3 =& \frac{\left(x_1^2-1\right)^2}{16(\rho+1)^7(\rho+2)^3}\Big[8\rho^6+40\rho^5-8\rho^4\left(x_1^2-7\right)-4\rho^3\left(3x_1^2+10\right)+\\
&+\rho^2\left(29x_1^2-169\right)+4\rho\left(11x_1^2-29\right)-4x_1^2+4\Big]\,,\\
g_4 =& -\frac{\left(x_1^2-1\right)}{96(\rho+1)^{10}(\rho+2)^4}\Big[12\rho^{10}\left(x_1^2-1\right)+8\rho^9\left(13x_1^2-10\right)-24\rho^8\left(3x_1^4-18x_1^2+2\right)+\\
&+\rho^7\left(-390x_1^4+744x_1^2+1392\right)+\rho^6\left(60x_1^6-465x_1^4-1147x_1^2+7030\right)+\\
&+3\rho^5\left(42x_1^6+569x_1^4-2728x_1^2+5615\right)-3\rho^4\left(131x_1^6-2126x_1^4+5326x_1^2-7489\right)+\\
&+\rho^3\left(-1164x_1^6+7329x_1^4-12824x_1^2+15491\right)-6\rho^2\left(85x_1^6-228x_1^4+149x_1^2-542\right)+\\
&+12\rho\left(30x_1^6-155x_1^4+246x_1^2-97\right)-4\left(3x_1^6-27x_1^4+41x_1^2+7\right)\Big]\,.
\end{aligned}
\tag{A.6}
$$

The results for $g_{ij}^{(0)}$ and $g_{ij}^{(3)}$ follow in a straightforward way and are given in section 3. We have checked that the other terms satisfy $g_{ij}^{(1)}=0$ and $g_{ij}^{(2)}=R_{ij}^{(0)}-\frac{1}{4}R^{(0)}g_{ij}^{(0)}$ in agreement with the general analysis in [12].

References

[1] S. Bhattacharyya, V.E. Hubeny, S. Minwalla and M. Rangamani, *Nonlinear fluid dynamics from gravity*, *JHEP* **02** (2008) 045 [arXiv:0712.2456] [SPIRES].

[2] O. Aharony, S. Minwalla and T. Wiseman, *Plasma-balls in large-N gauge theories and localized black holes*, *Class. Quant. Grav.* **23** (2006) 2171 [hep-th/0507219] [SPIRES].

[3] S. Lahiri and S. Minwalla, *Plasmarings as dual black rings*, *JHEP* **05** (2008) 001 [arXiv:0705.3404] [SPIRES];
S. Bhardwaj and J. Bhattacharya, *Thermodynamics of plasmaballs and plasmarings in $3+1$ dimensions*, *JHEP* **03** (2009) 101 [arXiv:0806.1897] [SPIRES];
K.-I. Maeda and U. Miyamoto, *Black hole-black string phase transitions from hydrodynamics*, *JHEP* **03** (2009) 066 [arXiv:0811.2305] [SPIRES];

JHEP08(2009)012

M.M. Caldarelli, O.J.C. Dias, R. Emparan and D. Klemm, *Black holes as lumps of fluid*, *JHEP* **04** (2009) 024 [arXiv:0811.2381] [SPIRES];
V. Cardoso and O.J.C. Dias, *Bifurcation of plasma balls and black holes to lobed configurations*, *JHEP* **04** (2009) 125 [arXiv:0902.3560] [SPIRES];
J. Bhattacharya and S. Lahiri, *Lumps of plasma in arbitrary dimensions*, arXiv:0903.4734 [SPIRES];
J. Evslin and C. Krishnan, *Metastable black saturns*, *JHEP* **09** (2008) 003 [arXiv:0804.4575] [SPIRES].

[4] S.B. Giddings, *High energy QCD scattering, the shape of gravity on an IR brane and the Froissart bound*, *Phys. Rev.* **D 67** (2003) 126001 [hep-th/0203004] [SPIRES].

[5] R. Emparan, G.T. Horowitz and R.C. Myers, *Exact description of black holes on branes*, *JHEP* **01** (2000) 007 [hep-th/9911043] [SPIRES].

[6] R. Emparan, G.T. Horowitz and R.C. Myers, *Exact description of black holes on branes. II: comparison with BTZ black holes and black strings*, *JHEP* **01** (2000) 021 [hep-th/9912135] [SPIRES];
M. Anber and L. Sorbo, *New exact solutions on the Randall-Sundrum 2-brane: lumps of dark radiation and accelerated black holes*, *JHEP* **07** (2008) 098 [arXiv:0803.2242] [SPIRES];
M.M. Anber, *AdS_4/CFT_3+gravity for accelerating conical singularities*, *JHEP* **11** (2008) 026 [arXiv:0809.2789] [SPIRES].

[7] T. Tanaka, *Classical black hole evaporation in Randall-Sundrum infinite braneworld*, *Prog. Theor. Phys. Suppl.* **148** (2003) 307 [gr-qc/0203082] [SPIRES].

[8] R. Emparan, A. Fabbri and N. Kaloper, *Quantum black holes as holograms in AdS braneworlds*, *JHEP* **08** (2002) 043 [hep-th/0206155] [SPIRES].

[9] J.F. Plebanski and M. Demianski, *Rotating, charged and uniformly accelerating mass in general relativity*, *Annals Phys.* **98** (1976) 98 [SPIRES].

[10] I. Zakout, *The C-metric black hole near the IR-brane in the AdS_4 space*, hep-th/0210063 [SPIRES].

[11] M. Henningson and K. Skenderis, *The holographic Weyl anomaly*, *JHEP* **07** (1998) 023 [hep-th/9806087] [SPIRES].

[12] S. de Haro, S.N. Solodukhin and K. Skenderis, *Holographic reconstruction of spacetime and renormalization in the AdS/CFT correspondence*, *Commun. Math. Phys.* **217** (2001) 595 [hep-th/0002230] [SPIRES].

[13] R. Emparan, *AdS/CFT duals of topological black holes and the entropy of zero-energy states*, *JHEP* **06** (1999) 036 [hep-th/9906040] [SPIRES].

[14] G. Compere and D. Marolf, *Setting the boundary free in AdS/CFT*, *Class. Quant. Grav.* **25** (2008) 195014 [arXiv:0805.1902] [SPIRES].

[15] S. de Haro, *Dual gravitons in AdS_4/CFT_3 and the holographic Cotton tensor*, *JHEP* **01** (2009) 042 [arXiv:0808.2054] [SPIRES].

[16] D. Marolf and M. Trodden, *Black holes and instabilities of negative tension branes*, *Phys. Rev.* **D 64** (2001) 065019 [hep-th/0102135] [SPIRES];
D. Marolf and S.F. Ross, *Stringy negative-tension branes and the second law of thermodynamics*, *JHEP* **04** (2002) 008 [hep-th/0202091] [SPIRES].

[17] P. Creminelli, A. Nicolis and R. Rattazzi, *Holography and the electroweak phase transition*, *JHEP* **03** (2002) 051 [hep-th/0107141] [SPIRES].

[18] A. Maccarrone and G. Milanesi, in progress.

JHEP08(2009)012